Mon. Not. R. astr. Soc. (1991) **251**, 508–521

Near-infrared imaging polarimetry of bipolar nebulae – II. GL 2591

N. R. Minchin,[1] J. H. Hough,[1] A. McCall,[1] C. Aspin,[2] S. S. Hayashi,[2] Takuya Yamashita[3] and M. G. Burton[4]

[1]*Division of Physical Sciences, Hatfield Polytechnic, Hatfield, Hertfordshire AL10 9AB*
[2]*Joint Astronomy Centre, 665 Komohana Street, Hilo, Hawaii 96720, USA*
[3]*National Astronomical Observatory, Mitaka, Tokyo 181, Japan*
[4]*Anglo-Australian Observatory, PO Box 296, Epping, NSW 2121, Australia*

Accepted 1991 April 12. Received 1991 April 11; in original form 1990 October 5

SUMMARY

High spatial resolution near-IR polarization and surface brightness images of the reflection nebulosity GL 2591 are presented. The *J*, *H* and *K* surface brightness images reveal two non-concentric 'loops' of nebulosity aligned with the high-velocity, blueshifted outflow from GL 2591 IRS. The polarization vector maps show a centro-symmetric pattern centred on GL 2591 IRS, indicating that it is illuminating a near-IR reflection nebula. Evidence is presented that implies GL 2591 IRS is surrounded by a dense disc or toroid of material. The observed increase in polarization with wavelength for the reflection nebulosity is interpreted as evidence for the presence of grains with a size distribution larger than that found in the diffuse ISM. Models giving the spatial dependence of linear polarization of scattered light for various scattering geometries are presented. A model for the blueshifted outflow, in which the two loops of nebulosity are the result of two discrete mass outbursts from GL 2591 IRS, is presented.

1 INTRODUCTION

Young stellar objects embedded in molecular clouds are characterized by mass outflow, usually observed as a bipolar high-velocity flow of molecular gas. The direction of the outflow is usually coincident with the direction of the magnetic field in the parent molecular cloud (Sato *et al.* 1985). The source itself is often obscured from direct view at optical wavelengths by a disc or toroid of dust grains whose axis is parallel to the outflow direction. Radiation from the source also preferentially escapes along the poles of the disc, illuminating the surrounding molecular cloud and producing a highly polarized reflection nebula.

GL 2591 IRS is an unresolved (less than 2 arcsec at 2.2 μm, Howell, McCarthy & Low 1981), very luminous (6×10^4 $L_\odot$, Lada *et al.* 1984) IR molecular cloud source which has been the subject of extensive investigation. The IR spectrum shows strong absorptions at 3.1 μm and 9.7 μm attributed to ices and silicates respectively (Willner *et al.* 1982).

The position angle of polarization is constant between 2 μm and 20 μm at $\sim 170°$. This direction is normal to the blueshifted outflow of high-velocity CO gas first detected by Lada *et al.* (1984). The redshifted outflow is extended to the north-east and hence the outflow is not observed to be bipolar. Within 100 arcsec of GL 2591 IRS, however, both the redshifted and blueshifted outflows are along an approximate east–west direction and therefore normal to the position angle of polarization (Yamashita *et al.* 1987).

The orientation of the magnetic field in the parent cloud is near to 60° (Sato *et al.* 1985). However this is rather poorly defined since the field star polarizations in the region of GL 2591 show a large range of polarization position angles. For many molecular outflow sources the position angle of polarization of the source is orthogonal to the direction of the cloud magnetic field (Sato *et al.*). In the case of GL 2591 IRS, although there is a difference of 110°, the uncertainty of defining the direction of the cloud polarization does not preclude it having the same characteristics as most other molecular cloud sources.

Mapping of the CS line emission by Yamashita *et al.* (1987) shows there is a dense disc or toroid around the IR source, with approximate extent 80 arcsec north–south and 50 arcsec east–west. Yamashita *et al.* (1987) also found that the 2.2-μm levels of polarization are larger in the east–west direction than the north–south direction.

Deep 1-μm CCD exposures and polarization maps have been presented by Lenzen (1987). These show that the reflection nebula is illuminated by GL 2591 IRS, with the eastern part of the nebula forming a cone-like structure with the star at its apex. Lenzen also finds an elongated feature along position angle $-115°$, which is the approximate position angle of the line along which an H_2O maser (White *et al.* 1975), an H II region (Campbell 1984) and the IR

source itself lie. Rolph & Scarrott (1988) have also produced a polarization map of GL 2591, with an effective wavelength close to 1 μm. In contrast to the results of Lenzen they find that the polarization pattern in the nebula is consistent with illumination from an obscured source centred 15 arcsec west and slightly to the south of the known IR source. They propose that the new source is a member of a cluster of highly obscured young stars.

Forrest & Shure (1986, hereafter FS) have presented near IR images of GL 2591 showing the presence at 1.6 μm and 2.2 μm of a bright loop which is aligned with the direction of the high-velocity blueshifted outflow and which they interpret as the outline of a bubble or cavity with GL 2591 IRS at its eastern edge. The radiation associated with the loop is assumed to arise from scattering of photons from GL 2591 IRS off dust grains at the surface of the cavity. Torrelles *et al.* (1989) have mapped the NH_3 emission from GL 2591, showing a cavity structure opening from GL 2591 IRS. More recently Burns *et al.* (1989) have published an image of GL 2591 at H that shows the presence of a second loop of emission beginning at the western edge of the first.

In this paper we present new, high spatial resolution, polarization and surface brightness measurements of GL 2591 made using an IR camera. Images are presented at J (1.25 μm), H (1.65 μm) and K (2.2 μm) each of 38×36 arcsec angular extent. The magnitude, degree of polarization and position angle of polarization along the line-of-sight to GL 2591 IRS at J, H and K are given. The line-of-sight extinction to the star is derived. Evidence for a disc around GL 2591 IRS is discussed. The wavelength dependence of polarization observed from the reflection nebulosity is examined and models for the outflow geometry are presented. This is the second in a series of papers examining the environs of bipolar outflow sources (see Minchin *et al.* 1990, hereafter Paper I).

2 OBSERVATIONS

The observations reported here were made at the 3.8-m United Kingdom infrared Telescope (UKIRT) using the common-user near-IR Camera (IRCAM, McLean 1987) and the IR Polarimeter (IRPOL) on Mauna Kea, Hawaii.* Observations were made on the nights of 1987 July 30–31 and 1989 September 14–15. The chip used was a Santa Barbara Research Centre (SBRC) 62×58 pixel InSb array with Direct Read-Out (Orias, Hoffman & Casselman 1986). Observations were made using standard J, H and K filters using the high-resolution 0.62-arcsec pixel^{-1} plate scale. Measurements of linear polarization are achieved by imaging through a warm achromatic half-waveplate (IRPOL) placed upstream of any oblique reflections and which can be rotated to four set positions, spaced apart by 22.5°. All observations were made in the stare mode with images taken of the object followed by a nearby area (70 arcsec north) of blank sky for flat-fielding, and a dark current image with the field completely blanked off. The FWHM of point sources was 1.2–1.5 arcsec for the 1987 July observations (H and K polarization images) and 0.8–1.0 arcsec for the 1989 September observations (surface brightness images and J polarization image).

*The UKIRT is operated by the Royal Observatory, Edinburgh on behalf of the UK Science and Engineering Research Council.

The procedures adopted for data reduction were as follows. The dark signal was subtracted from each frame and then the object frame was flat-fielded by dividing by a median-filtered flat-field frame. Finally the object frame was rescaled to the mean of the flat-field frame. Bad pixels were replaced by interpolating the data from adjacent pixels. As GL 2591 is a relatively compact reflection nebula in the north–south direction it was possible to sky subtract the object frame by taking a sky level from the object frame itself. The degrees of polarization and position angles of polarization were calculated in a standard way from the sky subtracted frames corresponding to the four waveplate positions (see Rayner *et al.* 1989 for further details of standard reduction procedures). Photometric observations of standard stars were used to flux calibrate the final images.

The efficiency of the polarimeter in the different wavebands was measured by observations of standard polarized stars and by observing unpolarized standard stars through a previously calibrated wiregrid polarizer placed upstream of the waveplate. This was found to be 89 per cent at J, 96 per cent at H and 97 per cent at K. The zero of position angle was established from observations of the polarized standard stars BN and Elias 16 with assumed position angles at K of 116° (Johnson *et al.* 1981) and 70° (Hough *et al.* 1988) respectively.

The SBRC array is well known to be slightly non-linear in its photon response over its full dynamic range (Hoffman 1987; McCaughrean 1988, 1989). A correction for non-linearity has been applied to the observations. From existing measurements made for this detector array, and on theoretical grounds (McCaughrean 1989), we believe any residual non-linearity errors to be less than 1 per cent.

3 RESULTS

Surface brightness images for GL 2591 at J, H and K are presented in Plates 1–4 respectively. The K image is displayed at both low and high contrast (Plates 3 and 4 respectively) to clearly show the structure of the bright and faint reflection nebulosity. The offsets are in arcsec from GL 2591 IRS. As GL 2591 IRS is saturated on the K image, its degree of polarization, position angle and magnitude at this wavelength were determined from an image of shorter exposure. The object 10 arcsec west and 10 arcsec south of GL 2591 IRS is a foreground star (Lenzen 1987). At all three wavelengths there is a bright 'loop' of radiation centred 6 arcsec to the west of the IR source (we shall call this the inner loop); this is the feature first noted by FS and is ~12 arcsec in diameter. Further to the west there is a second loop that seems to begin at the western edge of the inner loop and is of noticeably lower surface brightness (we shall call this the outer loop). This feature is ~14 arcsec in diameter, centred 19 arcsec west of the star and is observed at all three wavelengths. It was not seen by FS, as it is to the west of their mapped area, but is the same feature noted by Burns *et al.* (1989) on their H image.

Our high-resolution images clearly show the western edge of the inner loop resolved into two arcs of nebulosity at J, H and K, as noted by FS on their H and K images. Also clearly resolved are two 'knots' of nebulosity, one to the northwest and one to the southwest of GL 2591 IRS. The brightest arc of nebulosity of the inner loop has a surface brightness (in

mag arcsec^{-2}) of ~15.2 at *J*, ~13.3 at *H* and ~11.9 at *K*, whilst the outer loop has a typical surface brightness (in mag arcsec^{-2}) of ~16.6 at *J*, ~15.2 at *H* and ~14.0 at *K*. The inner loop is clearly the brightest of the two features at all wavelengths and both loops increase in surface brightness from *J* to *K*. The implications of the second loop for the 'bubble' hypothesis of FS are that the geometry of the outflow cannot be explained by a single spherical outflow. A discussion of the outflow geometry will be presented in Section 4.4.

There is some evidence from our *J* surface brightness image (Plate 1) of the elongated feature noted by Lenzen (1987) along azimuthal angle 245° (where azimuthal angle is from due north in the anticlockwise direction). This line also connects the southern most edges of the inner and outer loops. If this is a jet-like feature, then it is clearly along the wall of the outflow (as delineated by the near-IR loops of nebulosity). Comparing fig. 1 of Campbell (1984) to our near-IR images shows that the H II region they designate as source 1 is roughly situated along this jet-like feature (the line connecting the southern most edges of the inner and outer loops) and their source 2 is roughly situated along the line connecting the norther most edges of the inner and outer loops (both H II regions are within 5 arcsec of GL 2591 IRS). The obvious implication of this is that these two H II regions are situated close to, or coincident with, the walls of the outflow and are therefore likely to be produced by GL 2591 IRS, and not by other young stars, as originally proposed by Campbell (1984).

Figs 1, 2, and 3 display polarization vectors overlayed upon surface brightness contours for GL 2591 at *J*, *H* and *K* respectively. At *K* the chip was saturated at the position of GL 2591 IRS, and therefore the polarization vectors across this source are incorrect. At *H* the signal-to-noise was only satisfactory for accurate polarimetry on the IR source and the inner loop (the surface brightness signal-to-noise cut-off for each pixel was 6 for the *J* polarization image and 10 for the *H* and *K* polarization images). At *H* and *K* the polarization vectors form a strong centro-symmetric pattern around the IR source along the western (blueshifted) outflow, indicating that GL 2591 IRS is illuminating the IR reflection nebula. At *J* there are slight variations from a centro-symmetric pattern, especially in the region of the outer loop where the polarization vectors are somewhat aligned. This is consistent with the 1-μm map of Lenzen (1987).

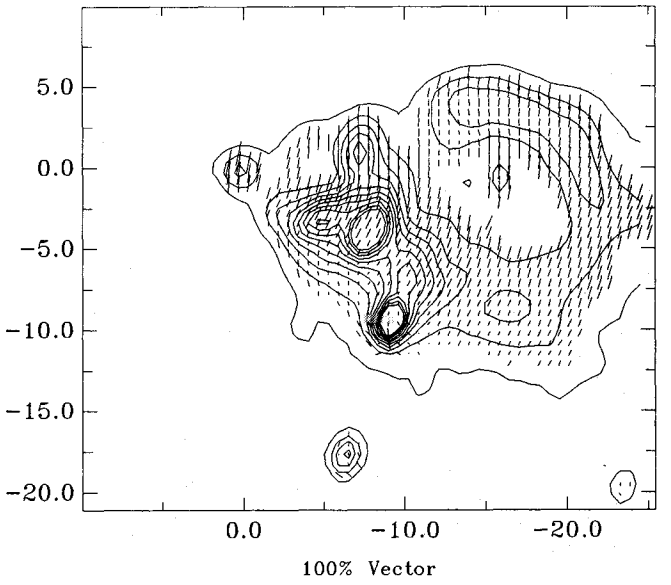

Figure 1. High-resolution (0.62 arcsec pixel^{-1}) imaging polarimetry of GL 2591 at *J*. The polarization vectors are superimposed upon the *J* surface-brightness contours. The base level contour is at 0.1 mJy arcsec^{-2} and the contour step is 0.1 mJy arcsec^{-2}. Offsets are in arcsec.

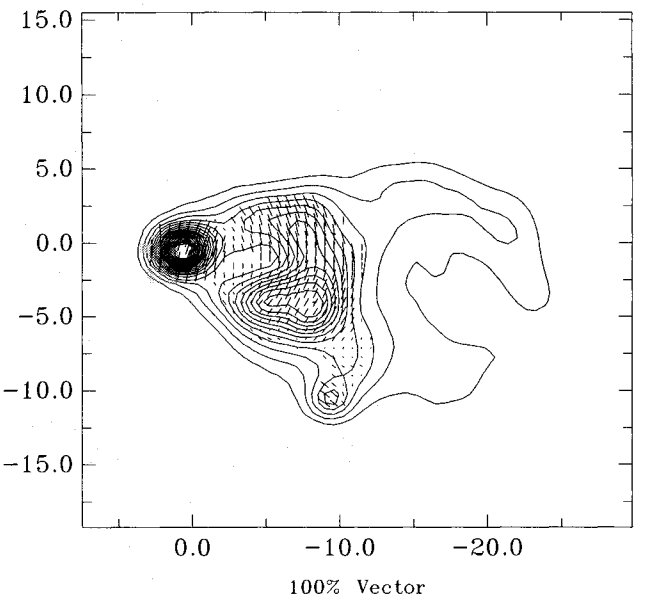

Figure 2. As for Fig. 1, but at *H*. The base level contour is at 0.4 mJy arcsec^{-2} and the contour step is 0.2 mJy arcsec^{-2}.

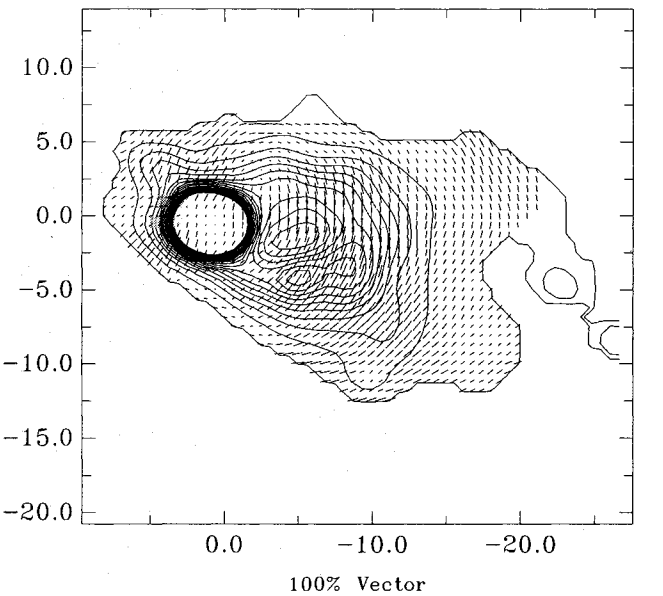

Figure 3. As for Fig. 1, but at *K*. The base level contour is at 1 mJy arcsec^{-2} and the contour step is 1 mJy arcsec^{-2}. The chip was saturated at the position of GL 2591 IRS, therefore the polarization vectors across this source are falsely low.

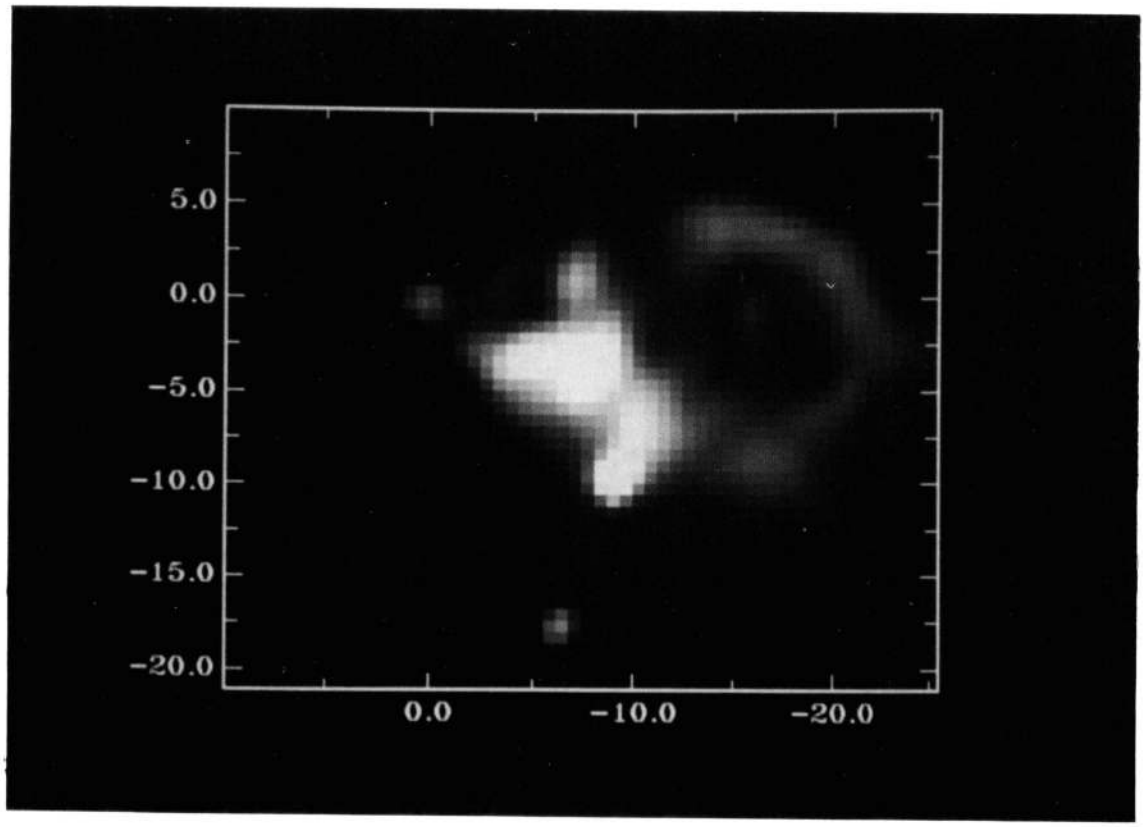

Plate 1. Surface brightness image of GL 2591 (0.62 arcsec pixel^{-1}) at *J*.

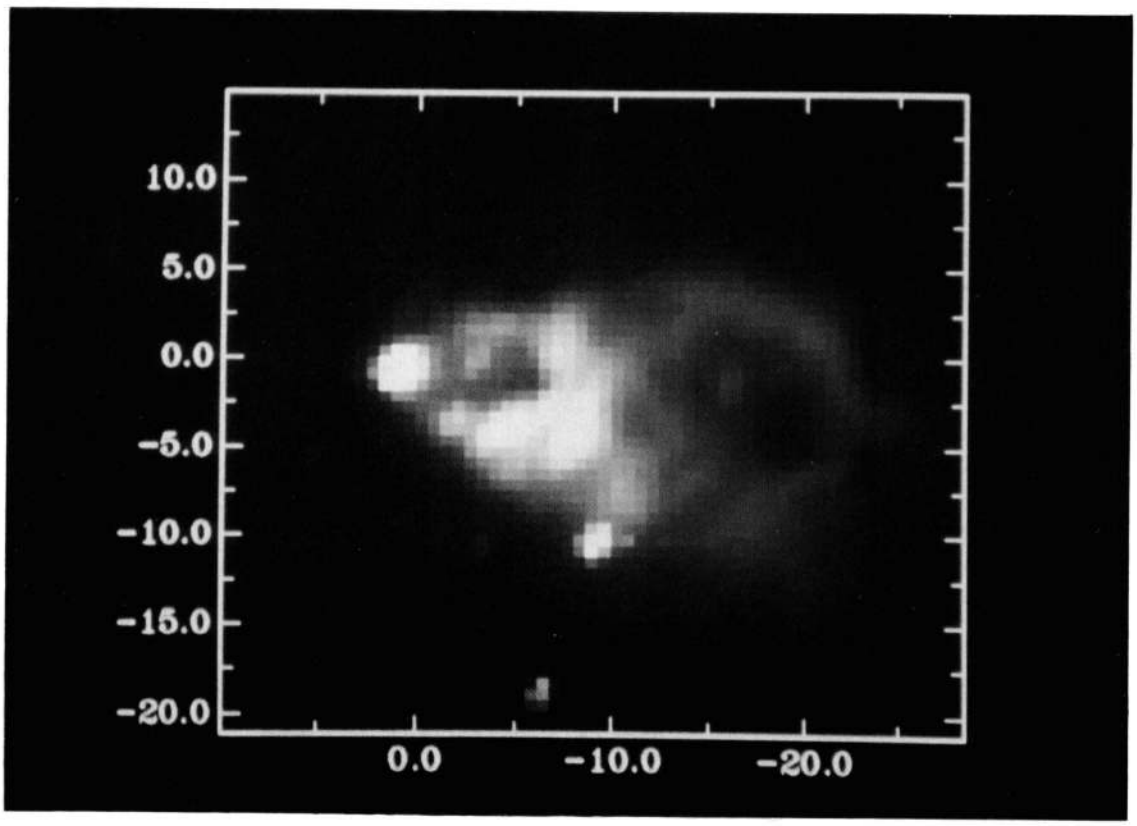

Plate 2. As for Plate 1, *H*.

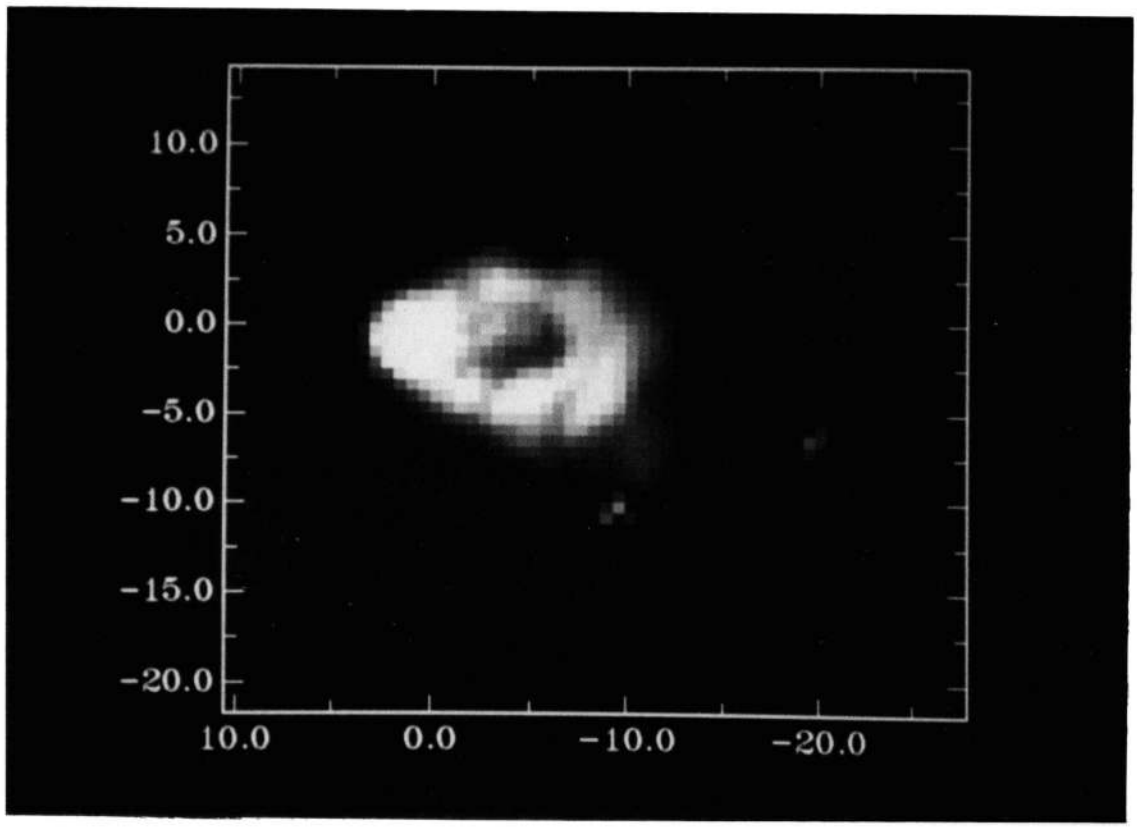

Plate 3. As for Plate 1, *K* at low contrast.

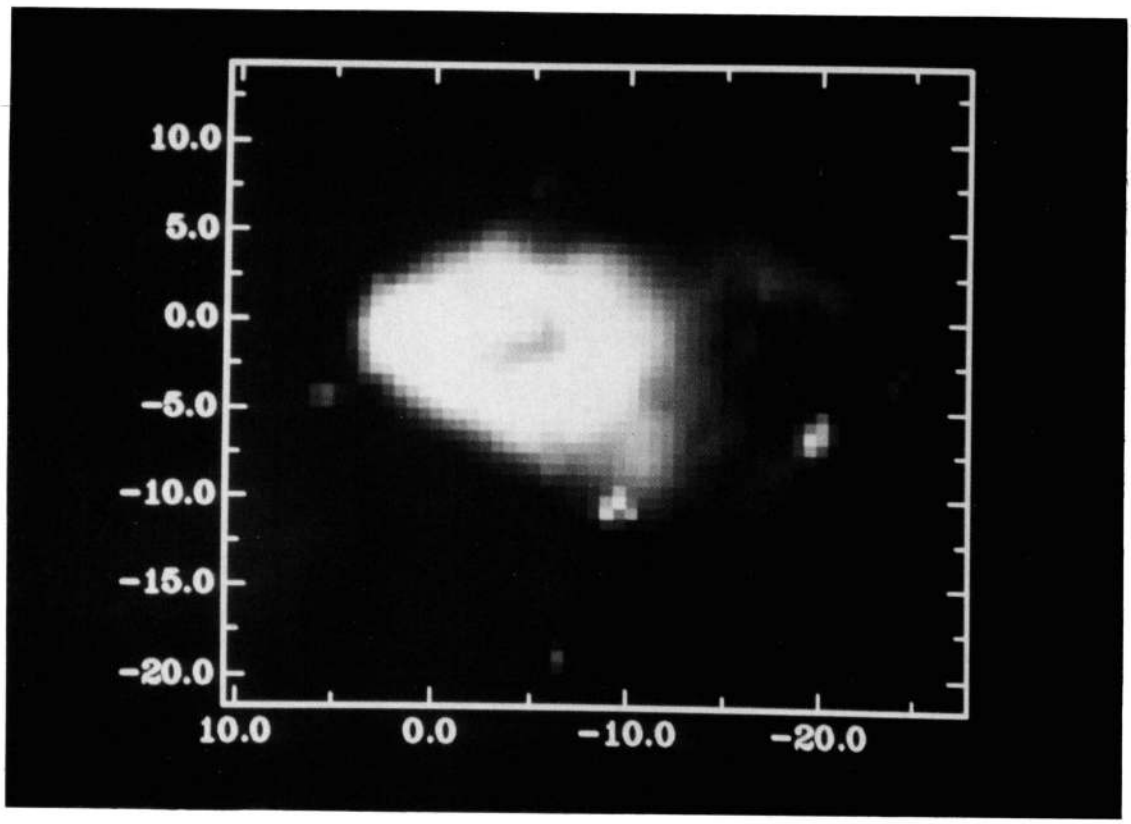

Plate 4. As for Plate 1, *K* at high contrast.

At J and H polarization values are between 10 per cent and 15 per cent in the inner loop region. At K they are slightly higher, up to 20 per cent around the inner loop and slightly larger towards the outer extent of the mapped region, consistent with the results of Yamashita *et al.* (1987) and Burns *et al.* (1989). At all three wavelengths the polarization vector pattern is consistent with GL 2591 IRS as the sole illuminator of the outflow region; there is no indication of a second illuminator to the southwest of the IR source, as proposed by Rolph & Scarrott (1988).

Table 1 gives the degree of polarization, position angle of polarization and magnitude for GL 2591 IRS at J, H, K. A software aperture of 6-arcsec diameter was used to avoid contamination from the limb of the inner loop. These apertures were achieved using a routine that sums the intensities of each pixel inside a circle of specifiable diameter in arcsec. Normally the error in an aperture polarimetry measurement is derived by performing the measurement numerous times and calculating the standard deviation of the resultant values. As only one array image was taken at each wavelength, this method is not applicable. It is also possible to estimate polarization value errors from photon statistics. However, as the near-IR flux in an aperture on a bright star is large, the statistical error of the polarization is very small. Also, this does not account for the polarization errors introduced by the data reduction, frame registration and polarization measurements, which dominate the statistical error. For this reason we derived a technique that involved slightly varying the position of the aperture on the object (± 1 pixel in either the x or y direction) and recalculating the percentage polarization and position angle of polarization. This was performed several times and the standard deviation found. The authors realize that the component measurements are correlated (as most of the pixels covered by each aperture are repeated) and therefore that normal statistics are not rigorously correct, but this method does give sensible error estimates.

The degree of polarization of radiation along the line-of-sight to the IR source is particularly high at J, 23.7 ± 1.4 per cent, decreasing to 13.3 ± 0.4 per cent at H and 9.7 ± 0.3 per cent at K. The degrees of polarization at H and K compare reasonably well with the numerous observations by other authors. Hough *et al.* (1989, hereafter HEA) found the degree of polarization at K to be 10.8 ± 0.1 per cent in a 7.8-arcsec beam, whilst Dyck & Capps (1978) found 12.7 ± 0.1 per cent and Burns *et al.* (1989) 9 ± 2 per cent, both using a 10-arcsec beam. Burns *et al.* (1989) found the degree of polarization at H to be 13 ± 2 per cent in a 10-arcsec beam and HEA observed 13.42 ± 0.13 per cent in a 7.8-arcsec beam.

The only previous observation at J was by HEA, which they found to be 8.1 ± 0.5 per cent in a 7.8-arcsec beam. This value is anomalously low and inconsistent with all the H and K observations as one would expect a higher degree of polarization for the star at J than at H or K, assuming the polarizing mechanism is either dichroic absorption by aligned grains along the line-of-sight to the IR source (e.g. HEA) or multiple scattering in a circumstellar disc (e.g. Elsasser & Staude 1978).

The star is relatively faint at J, having a magnitude of 14.4, increasing in brightness to 11.0 magnitudes at H and 6.1 magnitudes at K (calculated using a 6-arcsec aperture). These may be compared with the 13.3 magnitudes at J, 10.5 magnitudes at H and 6.14 magnitudes at K found by Burns *et al.* (1989) in a 10-arcsec aperture. The larger flux observed by them at the shorter wavelengths is probably due to flux contamination from the bright reflection nebulosity in the larger beam. Indeed when 10-arcsec diameter software apertures were used on our images similar values were found. The J–K and H–K and colours of GL 2591 IRS are 8.3 and 4.9 respectively. Such large colour gradients imply the star is highly reddened due to dust extinction along our line-of-sight, possibly due to a surrounding disc or toroid.

Table 1. Software aperture polarimetry and photometry of GL 2591 IRS.

λ	Aperture[a]	p[b]	θ[c]	M_{obs}[d]
J	6	23.7±1.4	171±1.8	14.4
H	6	13.3±0.4	167±1	11.0
K	6	9.7±0.3	171±1	6.1

[a]Software aperture diameter (in arcsec). [b]Percentage polarization. [c]Position angle of polarization, north through east (in degrees). [d]Observed magnitude (± 0.1).

4 DISCUSSION

4.1 Evidence for a disc around GL 2591 IRS

4.1.1 The line-of-sight extinction to GL 2591 IRS using the Hubble relation

One means of estimating the line-of-sight extinction to GL 2591 IRS is by applying the Hubble relation (Hubble 1922 and see Paper I for nomenclature and details). The results of applying the Hubble relation to GL 2591 at J, H and K are summarized in Table 2. It can be seen that at all three wavelengths the observed magnitudes of GL 2591 IRS are fainter than those derived from the Hubble relation. This implies the presence of optically thick material between the observer and GL 2591 IRS, but not between the observer and the nebulosity or GL 2591 IRS and the nebulosity. This differential extinction towards GL 2591 IRS is best

Table 2. Extinction to GL 2591 IRS using the Hubble relation.

λ	M_n[a]	θ[b]	M^*[c]	M_{obs}[d]	A(λ)[e]	A_V[f]
J	19.0	≥30	≤8.8	14.4	≥5.6	≥22
H	17.3	≥30	≤7.1	11.0	≥3.9	≥28
K	14.2	≥30	≤4.0	6.1	≥2.1	≥26

[a]3σ limiting surface brightness in mag arcsec^{-2} (± 0.2). [b]Angular distance in arcsec (± 0.6) to the edge of the reflection nebulosity. [c]Hubble magnitude (± 0.2) of GL 2591 IRS. [d]Observed magnitude (± 0.1) of GL 2591 IRS. [e]$M_{obs} - M^*$, the differential extinction to GL 2591 IRS in magnitudes (± 0.3). [f]The visual differential extinction in magnitudes, using $A_J = 0.26 A_V$, $A_H = 0.14 A_V$ and $A_K = 0.08 A_V$ (Steenman & The 1989).

explained by an optically thick disc or toroid of material around the star. The extinction due to this disc is found to be at least 5.6 mag at J, 3.9 mag at H and 2.1 mag at K. If the grain sizes are typical of the diffuse interstellar medium then, from the work of Steenman & The (1989), these values correspond to a visual extinction of at least 22–28 mag.

The value of θ used was 30 arcsec, which is the extent of our observations to the west of GL 2591 IRS, but the reflection nebulosity may extend beyond our mapped region. Yamashita *et al.* (1987) found that at K the reflection nebulosity extends to at least 60 arcsec to the west of GL 2591 IRS, and thus may extend to a similar angular distance at J and H. This implies our calculated visual extinction to GL 2591 IRS is a lower limit. The visual extinction to GL 2591 IRS has been estimated to be between 26 and 50 mag by Lada *et al.* (1984), and at least 22 mag by Lenzen (1987). A value of around 30 mag was derived by HEA using the hydrogen density and disc thickness estimated by Yamashita *et al.* (1987).

4.1.2 *The polarization vector maps*

Further evidence for a disc of material around GL 2591 IRS can be found from our K polarization vector map (Fig. 3). It can be seen that to the north-west, south-east and east of the star the polarization vectors are no longer centro-symmetric about this source. The vectors, particularly to the north and south of GL 2591 IRS, are directed along a position angle of between 150° and 170°, roughly along the plane of the dense molecular disc, as delineated by the CS observations of Yamashita *et al.* (1987) and roughly orthogonal to the outflow direction. This is not surprising if the star is surrounded by a dense disc, with a toroidal magnetic field, as in this case scattered light will have to pass through magnetically aligned grains, producing a component of polarization along the plane of the disc. As the disc is believed to be tilted so as to obscure IR radiation scattered from the eastern (redshifted) outflow, one would also expect the polarization vectors to the east of GL 2591 IRS to be somewhat aligned along the disc direction, which is apparently the case.

There is a distinct twist in the polarization vector pattern from 140–150° to the south-east of the star to 171° along the line-of-sight to GL 2591 IRS, returning to 140–150° to the north-west of the star. Somewhat similar twists are observed in the polarization vector patterns across the optical bipolar nebulae R&T CrA (Ward-Thompson *et al.* 1985), LkHα233 (Aspin, McLean & McCaughrean 1985) and the Serpens Nebula (Warren-Smith *et al.* 1987).

The twist may be due to the combination of polarizations produced from the scattering of radiation in the dense disc, where the position angle will vary according to the scattering angle (i.e. defined by the geometry of the disc) and by dichroic absorption where the position angle is expected to be along the plane of the disc (if there is a toroidal magnetic field).

It is also clear from Fig. 3 that the polarization values just to the north-west and south-east of the star are lower than along the outflow direction, with distinct 'null' polarization points to the north (centred roughly -3, $+4$ arcsec) and south (centred roughly $+2$, -4 arcsec) of GL 2591 IRS. These are suggestive of competing polarization mechanisms that cancel each other at certain points, again implying a combination of scattering and absorption by aligned grains within the disc. Similar null polarization points have been observed to the east and west of R Mon (Gething *et al.* 1982; Scarrott, Draper & Warren-Smith 1989) and have also been attributed to competing polarization mechanisms.

If the position angle of polarization for GL 2591 IRS, i.e. 171°, defines the plane of the disc then the null points would be expected to lie along a line of position angle 171°. But the null points actually define a line inclined by roughly 20–30° to the plane of the disc, i.e. a position angle of 140–150°. This, and the observed twist in the position angle of polarization vectors across the disc, imply one of two possibilities. First, that the disc is warped and correspondingly the toroidal magnetic field and direction of grain alignment are warped. Or secondly, that the disc is symmetric but the magnetic field (and hence the grain alignment) does not follow the plane of the disc.

Bastien & Menard (1988) have argued that just the multiple scattering of radiation in an optically thick disc can explain aligned vector patterns close to bipolar outflow sources and the relatively low polarization values observed along the plane of the disc compared to the outflow region. Such a model seems incapable, however, of producing the observed twist in the aligned vector pattern and the null polarization points without a highly contrived geometry or the additional effect of dichroic absorption from aligned grains.

There are three observations suggesting the existence of aligned grains along the line-of-sight to GL 2591 IRS. First, the observed shift of the 10-μm polarization peak to a longer wavelength than that of the extinction maximum (Aitken *et al.* 1988). Secondly, the constancy of the polarization position angle, within a few degrees of 171°, from 1 μm to 20 μm. Thirdly, Lonsdale *et al.* (1980) measured the circular polarization of GL 2591 IRS at 2.2 μm and concluded that it is best explained by dichroic absorption through a medium of aligned grains in which the direction of the grain alignment and the grain properties change along the line-of-sight.

4.1.3 *Colour cuts*

An $H-K$ colour image was produced and two radial cuts from GL 2591 IRS were taken, each of 20-arcsec extent. These are shown in Fig. 4. Cut A is roughly along the centre of the outflow direction (azimuthal angle of 270°) and cut B is offset from cut A by 30° in the clockwise direction (azimuthal angle of 240°). Both cuts indicate that, along the outflow direction, the nebula becomes increasingly blue with angular distance from the star, dropping by over 3 mag from $H-K \sim 4.9$ mag at the star to roughly $H-K \sim 1.5$–2 mag at an angular distance of 5–10 arcsec and then a decrease of only ~ 0.5 mag over the next 10–15 arcsec. Our cuts are in broad agreement with east–west parallel cuts of FS with the reddening decreasing roughly as $1/z$ for the angular distance range 0–20 arcsec. This increasing blueness of the nebula with radial distance from the illuminating star has been seen for many other reflection nebulae, such as the BN–KL region of OMC-1 (Paper 1) and GSS30 (Castelaz *et al.* (1985), and is most easily explained by high dust extinction around an illuminating star which decreases radially with angular distance, consistent with a dense disc of material around GL 2591 IRS.

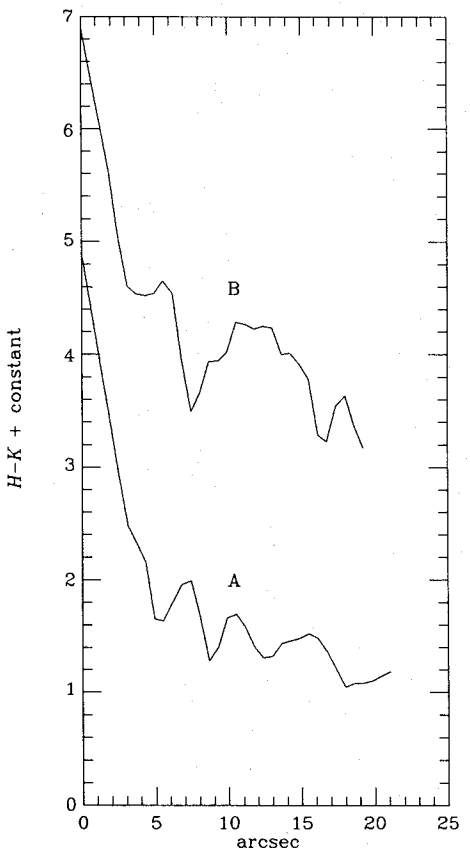

Figure 4. *H–K* colours along cut A (constant = 0) and cut B (constant = 2). Both cuts were taken radially outward from GL 2591 IRS.

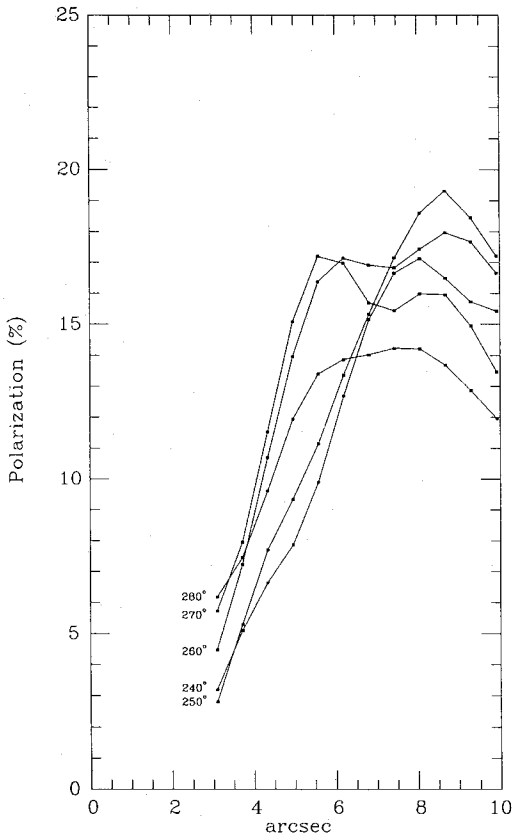

Figure 5. The radial dependence of *K* polarization values at azimuthal angles 240, 250, 260, 270 and 280°.

4.2 The wavelength dependence of polarization from the reflection nebulosity

To examine the wavelength dependence of polarization of scattered radiation from the blueshifted outflow region we calculated the ratio of polarization at *K* to that at *H* (P_K/P_H) along radial cuts from GL 2591 IRS. This ratio was found for each pixel between 3 and 10 arcsec from the star and these values averaged. These were found to be 1.57 ± 0.16, 1.59 ± 0.11 and 1.24 ± 0.13 along azimuthal angles 250°, 260° and 270° respectively. In fact P_K/P_H was found to be greater than unity at all points across the inner loop. If single Rayleigh scattering dominates then one would expect to observe roughly equal polarization values at *H* and *K* in the outflow region. The observations of Rolph & Scarrott (1988) show that the optical polarization from the blueshifted outflow region is less than 10 per cent. This is distinctly less than the 10–20 per cent observed by us in the near-IR and therefore implies the wavelength dependence noted by us is also apparent through to optical wavelengths.

The lower polarization observed at shorter wavelengths could be due to either progressively smaller degrees of multiple scattering or systematically larger scattering angles at the longer wavelengths. However, the discussion presented in Paper I concluded that multiple scattering can not have a significant effect on the wavelength dependence of polarization observed for reflection nebulae in the near-IR nor are scattering angles likely to increase significantly from *H* to *K*.

The presence of grains larger than those normally associated with the diffuse ISM will produce larger polarization at *K* than at *H* (Pendleton, Tielens & Werner 1990 and see Paper I). Fig. 12(b) from Pendleton *et al.* (1990) shows that, for a scattering angle of 60°, their 'large grain' model (with a grain size distribution of 0.225–0.8 μm) gives $P_K/P_H \sim 1.4$, consistent with the observed ratios. Therefore the presence of large grains must be considered the most likely explanation for the observed wavelength dependence of polarization.

4.3 The spatial dependence of polarization

Inspection of the polarization vector maps reveal marked variations in percentage polarization across the western (blueshifted) outflow (the 'loops'). The radial dependence of *K* polarization (between 3 and 10 arcsec from the star) at azimuthal angles 240, 250, 260, 270 and 280° are shown in Fig. 5. At each azimuthal angle the polarization increases with radial distance from GL 2591 IRS before reaching a plateau, beginning 6–7 arcsec from the star, roughly where the bright edge of the inner loop begins. A similar radial dependence was found at *J* and *H* over the same angular distance. As Gl 2591 IRS is over 8 mag brighter at *K* than at *J*, this implies that dilution from relatively unpolarized line-of-sight radiation from GL 2591 IRS itself is not significantly affecting the radial dependence of polarization in the near-IR.

We have averaged polarization values along radial lines of constant azimuthal angle from GL 2591 IRS, analogous to the method of Lenzen (1987) for the 1-μm continuum polarization around the bipolar outflow source L1551-IRS5. Averages were calculated over the radial distances 5-10 arcsec for both the H and K polarization maps (across the inner loop). The results and corresponding errors ($\pm 1\sigma$) are presented in Figs 6 and 7. This analysis was not used on the J data as it was not considered to be of sufficiently high quality.

The maximum K polarization average is at an azimuthal angle of between 260 and 270°, i.e. along the centre of the western (blueshifted) outflow, as delineated by the CO emission map of Lada *et al.* (1984), with polarization averages decreasing gradually for larger and smaller azimuthal angles. This dependence of polarization on azimuthal angle is very similar to that found by Lenzen (1987) for the reflection nebulosity around L1551-IRS5. The H polarization averages show the same general pattern, but the quality of the data is inferior to that at K. The following section describes models used to interpret the change in percentage polarization observed across the outflow region.

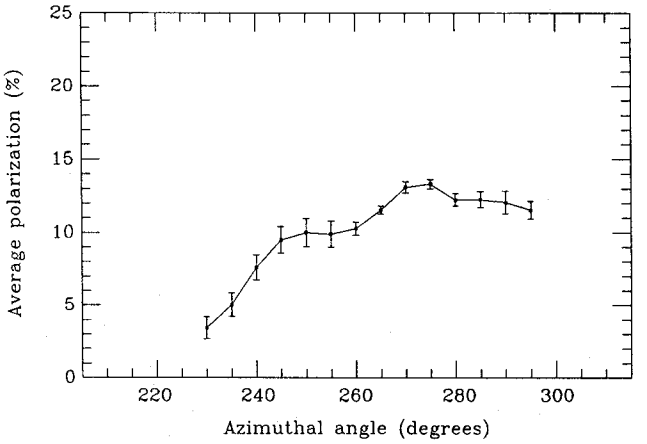

Figure 6. Average polarization values at H as a function of azimuthal angle. Azimuthal angle is positive in a clockwise direction on the sky (the error bars shown are the standard errors from the mean).

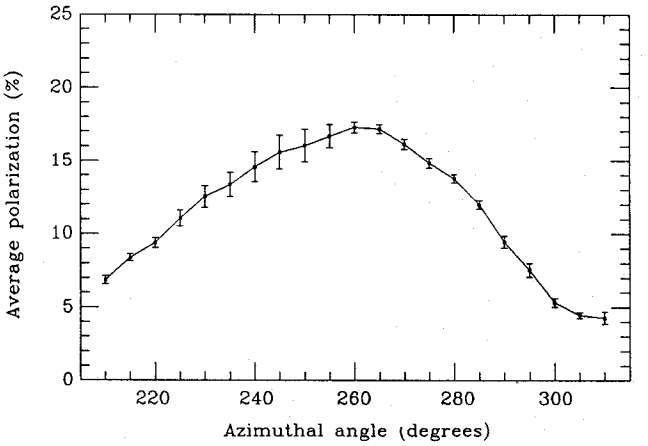

Figure 7. As for Fig. 6, but at K.

4.4 Modelling of the outflow geometry

4.4.1 Scattering geometries

We constructed computer models to simulate three different scattering geometries for the inner loop of radiation along the western (blueshifted) outflow direction.

(i) A spherical or 'bubble' geometry with GL 2591 IRS at its eastern edge (as proposed by FS). Hereafter this will be referred to as the sphere model.

(ii) A flat 'slab' at the end of an outflow of arbitrary shape (commonly assumed to be conical or parabolic) from GL 2591 IRS. Hereafter this will be referred to as the slab model. This geometry is similar to that proposed by Lenzen (1987) for L1551 and assumes the slab is circular in projection on the sky (to simulate the near-IR surface brightness distribution).

The surface brightness images (Plates 1-4) show the inner loop to be about 12 arcsec in diameter at all three near-IR wavelengths. This value was assumed for the projected angular size of the sphere or slab onto the plane of the sky.

(iii) For the third scattering geometry it was assumed that the outer loop of radiation represents the end of the outflow. Scattering is from the surface of a conical outflow cavity, with GL 2591 IRS at its apex. Hereafter this will be referred to as the cone model. The observation that the outer loop is ~ 14 arcsec in diameter and 19 arcsec from GL 2591 was used to calculate the opening angle of the outflow for different inclinations from the plane of the sky.

Schematic representations of the sphere, slab and cone models are shown in Fig. 8. For all three models we assume that scattering is single and that flux from the star drops as r^2. The inclination of the outflow from the plane of the sky was varied using a simple coordinate shift.

4.4.2 The sphere model

We examined two different scenarios for scattering from a spherical outflow. First, scattering from the walls of a spherical cavity (assuming there is no extinction within the cavity), so the resultant polarized intensity at any point is the sum of the polarized intensities from the front and back surfaces of the sphere along the line-of-sight (surface scattering). Secondly radiation is scattered from all points along our line-of-sight enclosed by the walls of the sphere (volume scattering). As the near-IR surface brightness distribution shows roughly circular loops to the west of the star, then if the outflow is spherical, it must be inclined close to the plane of the sky (if the outflow were inclined close to the line-of-sight then the star would appear to be inside the loops of radiation).

The radial dependence of percentage polarization produced by Rayleigh scattering for various azimuthal angles and outflow inclinations was calculated for the sphere model assuming both surface and volume scattering. Some representative results are shown in Fig. 9.

The sphere models produce polarization values that are far too high, starting as low as 15 per cent and rising to nearly 90 per cent for the surface scattering model, and starting at 55 per cent and rising to over 90 per cent for the volume scattering model. Rates of increase with radial distance are also much higher than observed and the constancy of polari-

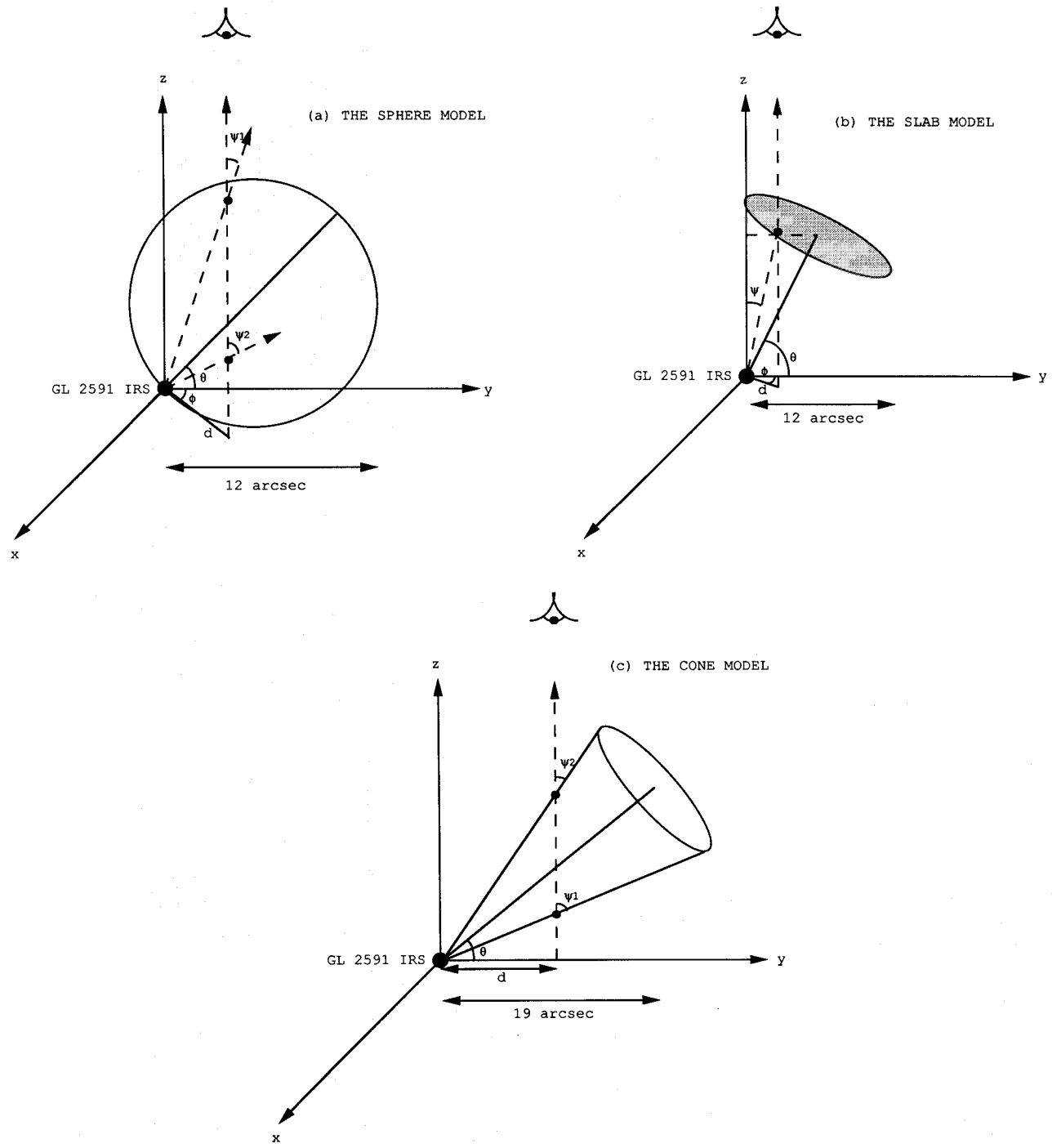

Figure 8. Schematic representations of (a) the sphere model, (b) the slab model and (c) the cone model. For each model the z axis is the line-of-sight to GL 2591 IRS, the y axis is along the centre of the outflow direction and the x–y plane is the plane of the sky. θ is the inclination of the outflow from the plane of the sky. For the slab model, ψ is the scattering angle from the slab itself. For the sphere and cone models, ψ_1 and ψ_2 are the scattering angles from the front and back surfaces of the outflow geometry. ϕ defines the azimuthal angle of radial cuts from GL 2591 IRS and d is the projected distance of the scattering point along the cut.

zation between 6 and 10 arcsec from GL 2591 IRS is not reproduced. Similarly high percentage polarization values were found whatever the inclination of the outflow from the plane of the sky.

Average polarization values were calculated along lines of constant azimuthal angle between 5 and 10 arcsec angular distance from the origin of the outflow (in 0.62 arcsec steps) to simulate the observed results. These are shown in Fig. 11 for both the surface and volume scattering sphere models. Both surface and volume scattering give dependences that are totally opposite to the observations. There is always a minimum along the centre of the outflow direction, with polarization averages gradually increasing for azimuthal angles progressively closer to the projected outer edges of the

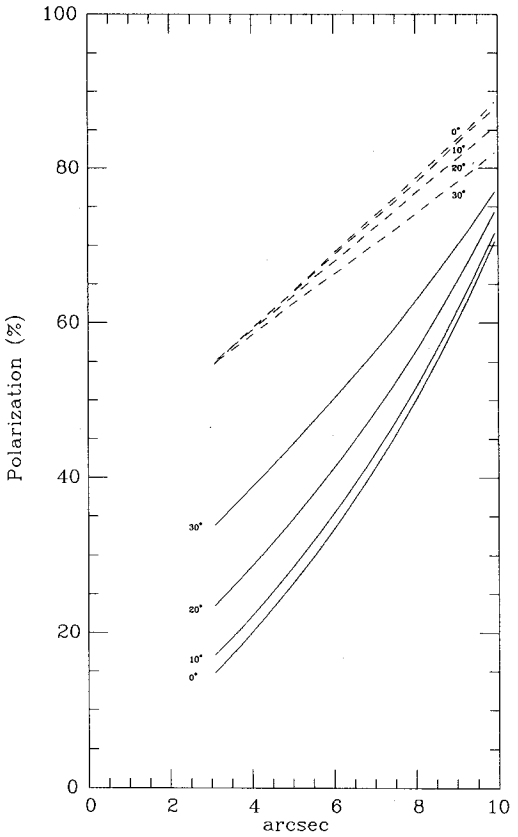

Figure 9. The radial dependence of polarization values calculated using the sphere model (assuming Rayleigh scattering) along the centre of the outflow direction and the inclination of the outflow from the plane of the sky are labelled. Values were calculated from the model assuming both surface scattering (solid lines) and volume scattering (dashed lines).

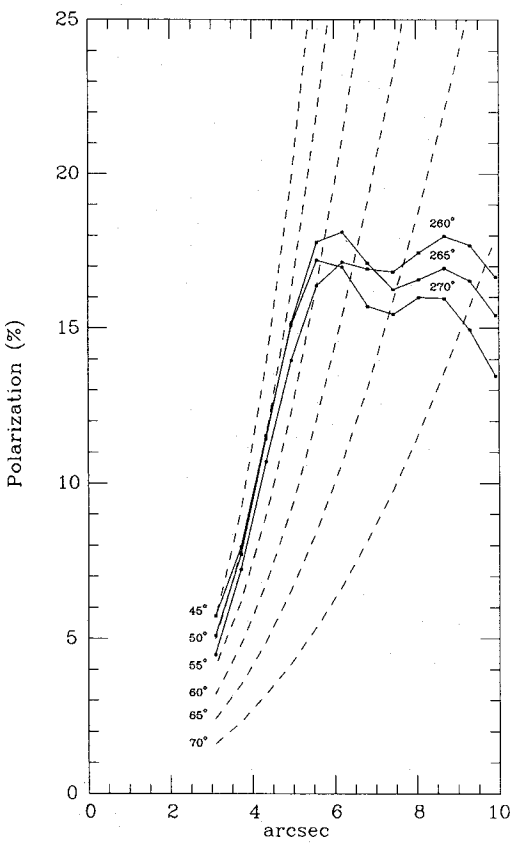

Figure 10. Polarization values along the centre of outflows for various inclinations from the plane of the sky (45–70°) calculated for Rayleigh scattering using the slab model (dashed lines) overlayed upon the observed K polarization values along the centre of the western (blueshifted) outflow (azimuthal angles 260, 265 and 270°).

outflow. The polarization averages are far in excess of those observed, 45–65 per cent for surface scattering and 72–82 per cent for volume scattering.

4.4.3 *The slab model*

Fig. 10 displays polarization values along the centre of outflows for various inclinations from the plane of the sky (45–70°) using the slab model (dashed lines) overlayed upon the observed values at K along the centre of the western outflow (azimuthal angles of 260, 265 and 270°). The rate of increase closely approximates the observations for an outflow inclined between 50 and 55° from the plane of the sky up to 6 arcsec from GL 2591 IRS, but the model does not account for the approximately constant polarization observed beyond 6 arcsec.

As for the sphere model, average polarization values were calculated along lines of constant azimuthal angle between 5- and 10-arcsec angular distance from the origin of the outflow. These are shown in Fig. 11. The slab model gives the same basic dependence as that observed for GL 2591, with the maximum along the centre of the outflow direction and polarization averages gradually decreasing for azimuthal angles progressively closer to the outer edges of the outflow. The calculated values are most similar to those observed for an outflow inclined between 65 and 70° from the plane of the sky.

As the slab model overestimates the polarization values observed beyond 6 arcsec from the star, we have recalculated the average polarization along lines of constant azimuthal angle for radial distances between 3 and 6 arcsec. Fig. 12 shows the averages of the observed polarization values at K and Fig. 13 shows the calculated averages for the slab model together with the observed values at K (dashed line). It can be seen that the same basic pattern produced by averaging the data over a more extended radial distance is preserved. Along the centre of the outflow direction (0°) the averages are consistent with an outflow direction inclined from the plane of the sky by between 50 and 55°, in agreement with the radial dependence of polarization.

4.4.4 *The cone model*

Fig. 16 displays polarization values along the centre of outflows for various inclinations from the plane of the sky using the cone model (short dashed lines). These are overlayed upon the observed values at K along the centre of the western outflow (azimuthal angles of 260, 265 and 270°). Due to the constancy of the scattering angle along the cavity walls, the resultant polarization at each point along the centre of the outflow is also constant. Therefore this model

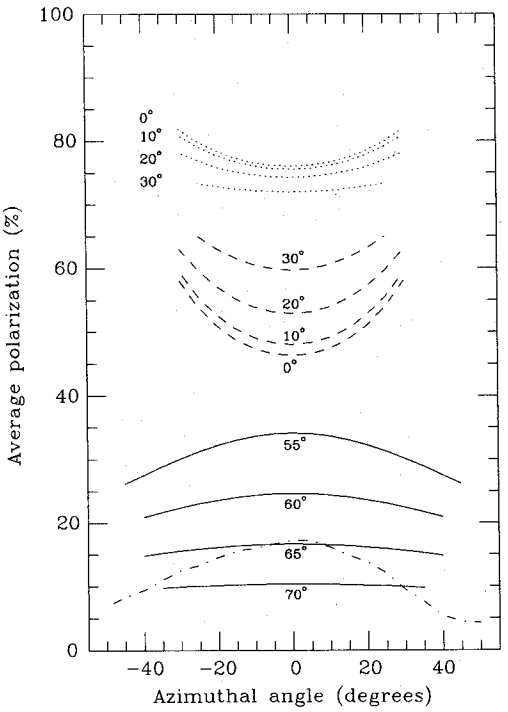

Figure 11. Average polarization values along radial lines of constant azimuthal angle, over the angular distance 5–10 arcsec from an illuminating star, using the slab model (solid lines), the surface scattering sphere model (dashed lines) and the volume scattering sphere model (dotted lines). The average polarization values at K are also plotted (dot-dash line). The zero of azimuthal angle is along the centre of the outflow direction and the labels on the curves are the inclinations of the outflows from the plane of the sky (in degrees).

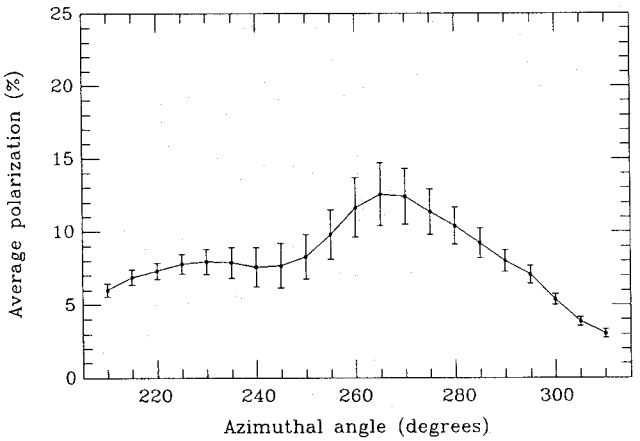

Figure 12. Average polarization values at K along radial lines of constant azimuthal angle from GL 2591 IRS over the angular distance 3–6 arcsec from the star (the error bars shown are the standard errors from the mean).

has the advantage over the slab model in that it is able to reproduce the approximately constant polarization for angular distances greater than 6 arcsec from GL 2591 IRS. Assuming Rayleigh scattering, an outflow inclined by ~65° from the plane of the sky is implied.

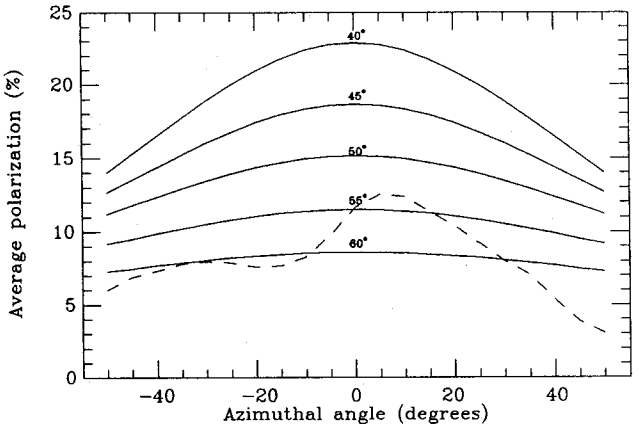

Figure 13. Average polarization values along radial lines of constant azimuthal angle, over the angular distance 3–6 arcsec from an illuminating star, calculated for Rayleigh scattering using the slab model (solid lines). The average polarization values at K are also plotted (dot-dash line). The zero of azimuthal angle is along the centre of the outflow direction and the labels on the curves are the inclinations of the outflows from the plane of the sky (in degrees).

Obviously the steadily decreasing polarization for angular distances less than 6 arcsec from GL 2591 IRS is not predicted from the cone model. As we have already discussed in Section 4.3, significant dilution of the polarization for this region by relatively unpolarized line-of-sight radiation from GL 2591 IRS is unlikely. Another, more probable, explanation is as follows.

Fig. 4 shows that the $H-K$ colour along the outflow direction decreases by more than three magnitudes over the first 5–6 arcsec from GL 2591 IRS, at which point it remains roughly constant (see Section 4.1.3). This point is also where the polarization 'plateau' begins. We have already attributed the high reddening of radiation observed close to, and along the line-of-sight to GL 2591 IRS to dust extinction in a dense disc. Therefore, the radiation observed close to GL 2591 IRS is likely to be a combination of multiple scattered radiation from the disc (and therefore relatively lowly polarized and at a variety of position angles) and single scattered radiation from the outflow region. The addition of the multiple scattered polarization components from the disc will effectively dilute the single scattered component. This effect will be most pronounced close to the star and will thus result in the lowest polarization values close to the star, as observed. The high inclination of the outflow from the plane of the sky (implied from the modelling) and the fact that radiation from the redshifted outflow is highly obscured are both consistent with the presence of an inclined disc.

4.4.5 *The effect of large grains*

So far our modelling has assumed Rayleigh scattering, but, as discussed in Section 4.2, the observed wavelength dependence of near-IR percentage polarization from the reflection nebulosity can be explained by the presence of grains larger than those found in the diffuse ISM. Examination of fig. 12(a) from Pendleton *et al.* (1990) indicates that at 2.2 μm the 'large grain' model gives polarization values a factor of roughly 2–3 (as one goes from small to large scattering

angles) times lower than those produced by Rayleigh scattering. This implies, if there are similar large grains in GL 2591, that the values calculated from our Rayleigh scattering models overestimate the expected K polarization values from the reflection nebulosity by a similar amount.

We have examined the effect of large grains on both the slab and cone models. Using values taken from fig. 12(a) of Pendleton *et al.* (1990), we repeated our calculations of the radial dependence of polarization and the average percentage polarization as a function of azimuthal angle (between 3 and 6 arcsec from GL 2591 IRS) for the slab model. Fig. 14 displays the radial dependence of polarization along the centre of the outflow for various inclinations from the plane of the sky (30–60°). There is no inclination of the outflow for which this model simulates the observed radial dependence, as closely as the Rayleigh scattering model. An outflow inclined by around 30° from the plane of the sky gives the closest fit, but the slab model is still unable to produce the observed polarization values for angular distances greater than 6 arcsec from the star. Fig. 15 displays the variation of average polarization values at K as a function of azimuthal angle for various inclinations of the outflow from the plane of the sky (30–60°). For reference the observed K dependence is plotted as a dashed line. Along the centre of the outflow the observations are most consistent with an outflow inclined by around 30°. This is distinctly lower than the value of 50–55° calculated assuming Rayleigh scattering (see Section 4.4.3).

In the slab model the increase in polarization between 3 and 6 arcsec from the source is produced by an increase in scattering angle. As already noted, the Pendleton *et al.* 'large grain' model produces larger values of P_K/P_H for larger scattering angles, hence P_K/P_H is expected to increase with radial distance from GL 2591 IRS. We find no evidence for such an increase. Hence, if large grains are responsible for the increase in polarization at the longer wavelengths, the scattering of radiation from a slab does not appear to be an appropriate model for GL 2591.

In contrast, the cone model (with scattering along the cone walls) produces a constant scattering angle and can thus readily explain the constancy of P_K/P_H across the outflow. We repeated our calculations of the radial dependence of polarization for the cone model, but now taking into account the effect of large grains. The results are shown in Fig. 16 (long dashed lines). An outflow inclined by ~55–60° from the plane of the sky is implied. For such an inclination, the opening angle of the outflow will be ~25–30°. From the 'large grain' modelling of Pendleton *et al.* (1990) a value of $P_K/P_H \sim 1.4$ is expected for the scattering from such an outflow, in agreement with the observed ratios (see Section 4.2).

Of course Rayleigh particles give an almost isotropic angular dependence of the scattering cross-sections, whereas Mie scattering (from large particles) is forward throwing. This means that Mie scattering will produce a larger scattered flux from points on the front surface of the cone than from the back surface. The above calculations of the radial dependence of polarization for the cone model, taking into account the effect of large grains, does not account for the different scattering cross-sections from the front and

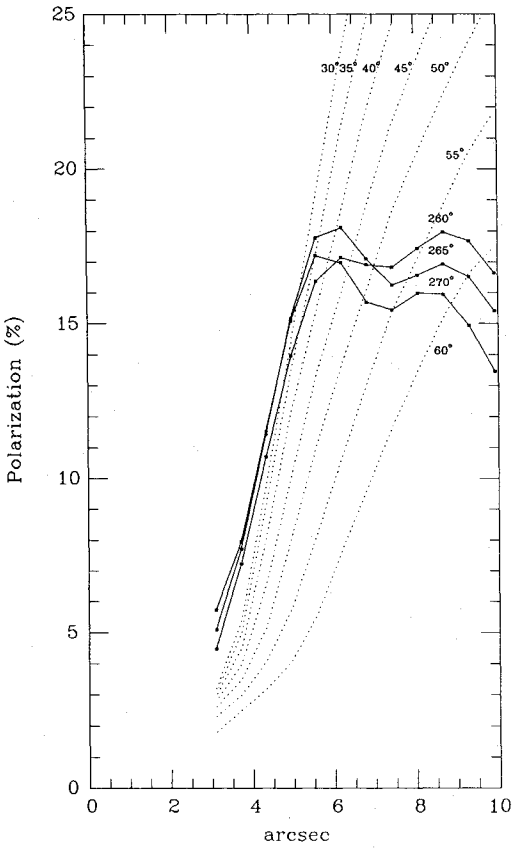

Figure 14. The radial dependence of K polarization values along the centre of the outflows of various inclinations from the plane of the sky calculated using the slab model taking into account the effect of large grains. Polarization values (dotted lines) are overlayed upon the observed K polarization values along the centre of the western (blueshifted) outflow (azimuthal angles of 260, 265 and 270°). The labels on the curves are the inclinations of the outflows from the plane of the sky (in degrees).

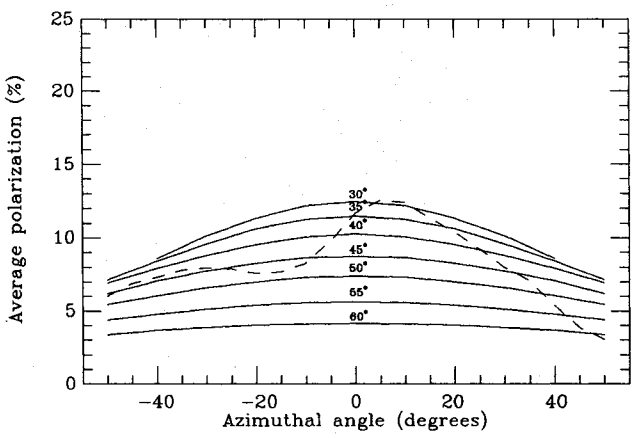

Figure 15. Average polarization values at K along radial lines of constant azimuthal angle from an illuminating star, calculated using the slab model (solid lines) taking into account the effect of large grains. The observed average polarization values at K are also plotted (dot-dash line). The zero of azimuthal angle is along the centre of the outflow direction and the labels on the curves are the inclinations of the outflows from the plane of the sky (in degrees).

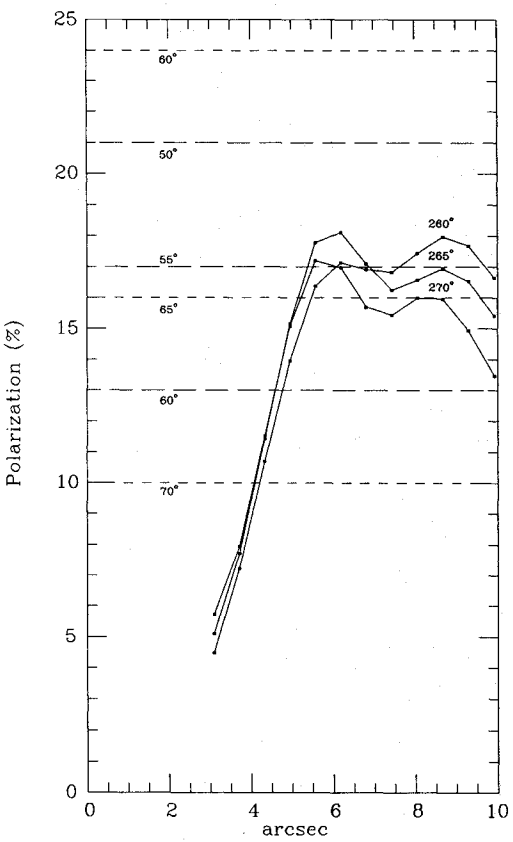

Figure 16. Polarization values along the centre of outflows for various incliantions from the plane of the sky (labelled) using the cone model. These are overlayed upon the observed values at K along the centre of western (blueshifted) outflow (azimuthal angles of 260, 265 and 270°). Calculations assuming Rayleigh scattering (short dashed lines) and those taking into account the effect of large grains (long dashed lines) are included.

back surfaces. This means that the values plotted in Fig. 16 will be slight overestimates.

We can make the following conclusions. Despite the attraction of a spherical outflow, as first proposed by FS to explain the observed 'loop' structure, we are unable with such a geometry to reproduce either the radial or azimuthal dependence of polarization across the western outflow. While the slab model can reproduce the radial dependence of polarization close to the source and the azimuthal dependence of polarization, it cannot explain the approximate constancy of polarization beyond 6 arcsec. It is also difficult with the slab model to explain the constant ratio of P_K/P_H. The cone model, however, is able to explain the radial dependence of polarization and the constancy of P_K/P_H and we conclude that the scattering of radiation from large grains along the walls of a conical cavity, inclined by ~ 55–65° from the plane of the sky, represents the most likely geometry for the western (blueshifted) outflow from GL 2591 IRS.

4.5 An explanation for the 'loops'

We propose that the two, non-concentric, loops of nebulosity are the result of two discrete mass outbursts from GL 2591 IRS. The larger projected angular size of the outer loop compared to the inner loop (15–18 arcsec compared to 12 arcsec) and its larger angular separation from the star are consistent with this hypothesis. The higher surface brightness of the inner loop compared to the outer loop, at all observed near-IR wavelengths, is consistent with it being physically closer to the star and of higher density. How a young star could undergo a second period of mass ejection, requiring a total energy of 10^{44}–10^{47} ergs (Bally & Lada 1983), is unclear, but recurrence of energetic mass loss is not unknown in more evolved stars (e.g. recurrent novae).

Assuming the outflow is inclined from the plane of the sky by ~ 55° and using the line-of-sight velocity component of the CO gas of $\Delta V/2 = 21$ km s^{-1}, observed for GL 2591 by Bally & Lada (1983), then one can derive an estimate of the true outflow velocity (26 km s^{-1}). As the projected separations (in the plane of the sky) of the centres of the inner and outer slabs, from GL 2591 IRS, are 6 arcsec and 19 arcsec respectively, we can also derive an estimate for their true separations from the star ($\sim 3\times10^{12}$ km and $\sim 9\times10^{12}$ km respectively). We can now derive a dynamical time-scale for an outflow to produce the inner and outer slabs of $\sim 4\times10^{3}$ yr and $\sim 1\times10^{4}$ yr respectively, implying a gap or quiescent phase of $\sim 6\times10^{3}$ yr between the beginning of the first outflow phase and the beginning of the second. Such time-scales are consistent with the estimated total duration of the energetic outflow phase of young stellar objects (10^{4}–10^{5} yr) derived by Bally & Lada (1983).

The loop-like appearance produced by the two outflow phases could be due to the method of outflow collimation. Basically, two methods of collimating the outflow have been proposed. First the wind leaving the stars surface is initially isotropic and is then collimated or confined by a circumstellar disc/toroid (e.g. Snell, Loren & Plambeck 1980) or a larger molecular disc (e.g. Canto *et al.* 1981). Secondly, mass is initially ejected anisotropically, possibly by a centrifugally-driven hydromagnetic wind (e.g. Pudritz & Norman 1983) or by the unwinding of the 'magnetic twist' (in the helical field perpendicular to the disc), created by the rotation of the disc, that drives out mass in the polar directions (Uchida & Shibata 1984).

If the first method is correct then mass initially ejected as an isotropic stellar wind may be channelled by the pressure distribution of the disc. The outflow will be refracted into two anti-parallel annular streams, with mass flowing along the surface of the cavity walls (Canto & Rodriguez 1980; Canto *et al.* 1981). If the outflow phases were distinctly shorter than the quiescent period between them, then the resultant morphology would be the loop or 'smoke-ring' structure observed.

The second collimation method may also be applicable. The Uchida & Shibata model has been proposed for L1551 by Kaifu (1987) and Uchida *et al.* (1987), whereby mass outflow is confined in paraboloid-shaped cavity walls. Again if the outflow phases were distinctly shorter than the quiescent period between them, then a smoke-ring structure would be produced.

Both methods of collimating the outflow appear capable of producing the observed morphology of GL 2591, but only if the outflow is produced by two discrete outbursts from GL 2591 IRS. The first outflow phase will have been responsible for producing the approximately conical cavity, with the outer loop delineating the end of the outflow.

5 CONCLUSIONS

High-resolution polarization vector maps at *J*, *H* and *K* show a centro-symmetric pattern to the west of GL 2591 IRS, along the blueshifted outflow region, indicating it is illuminating a near-IR reflection nebula. Surface brightness maps at *J*, *H* and *K* show there to be two non-concentric 'loops' of nebulosity aligned with the blueshifted outflow.

There is strong evidence for the existence of a disc or toroid of material around GL 2591 IRS, such evidence includes:

(i) The wavelength independence of the position angle of polarization along the line-of-sight to GL 2591 IRS and its orientation perpendicular to the outflow axis – both consistent with radiation being polarized by transmission through grains aligned by a toroidal magnetic field in a surrounding disc.

(ii) The position angles and low levels of polarization observed to the north-west, south-east and east of GL 2591 IRS – consistent with a combination of scattering and dichroic absorption by aligned grains in a disc.

(iii) The high differential extinction to GL 2591 (22–28 visual magnitudes) found using the Hubble relation – indicating the presence of optically thick material between the observer and GL 2591 IRS, but not between the observer and the reflection nebulosity or GL 2591 IRS and the reflection nebulosity.

(iv) The high near-IR red colour excess along the line-of-sight to GL 2591 IRS ($J-K=8.3$, $H-K=4.9$) which decreases radially with angular distance along the outflow direction – implying high extinction to the star which decreases radially in the outflow direction.

Polarization values across the western (blueshifted) outflow region are observed to increase from 1.65 μm to 2.2 μm, this is best explained by the presence of grains with a size distribution larger than that found in the diffuse ISM. Modelling of the observed spatial dependence of polarization for the western outflow region implies that the scattering geometry is not a 'sphere' or a 'slab' (circular in projection on the plane of the sky). Instead the scattering of radiation from the walls of a conical outflow cavity, inclined between 55 and 65° from the plane of the sky, is able to reproduce the roughly constant polarization observed for angular distances greater than 6 arcsec from GL 2591 IRS. This 'cone' model is also able to explain the approximate constancy of the ratio of polarization values at *H* to *K* with angular distance from GL 2591 IRS. We propose that the two 'loops' of nebulosity are the result of two discrete mass outbursts from GL 2591 IRS.

ACKNOWLEDGMENTS

We thank the staff of the UKIRT for their help with the observations. We acknowledge PATT for the allocation of telescope time and travel funds. NRM acknowledges the receipt of an SERC studentship. Mark McCaughrean, John Rayner, Jeremy Bailey and Chris Brindle are thanked for their advice and comments.

REFERENCES

Aitken, D. K., Roche, P. F., Smith, C. H., James, S. D. & Hough, J. H., 1988. *Mon. Not. R. astr. Soc.*, **230,** 629.
Aspin, C., McLean, I. S. & McCaughrean, M. J., 1985. *Astr. Astrophys.*, **144,** 220.
Burns, M. S., Hayward, T. L., Thronson, H. A. & Johnson, P. E., 1989. *Astr. J.*, **98,** 659.
Bally, J. & Lada, C. J., 1983. *Astrophys. J.*, **265,** 824.
Bastien, P. & Menard, F., 1988. *Astrophys. J.*, **326,** 334.
Campbell, B., 1984. *Astrophys. J.*, **287,** 334.
Canto, J. & Rodriguez, L. F., 1980. *Astrophys. J.*, **239,** 982.
Canto, J., Rodriguez, L. F., Barral, J. F. & Carral, P., 1981. *Astrophys. J.*, **244,** 102.
Castelaz, M. W., Hackwell, J. A., Grasdalen, G. L., Gehrz, R. D. & Gullixson, G., 1985. *Astrophys. J.*, **290,** 261.
Dyck, H. M. & Capps, R. W., 1978. *Astrophys. J. Lett.*, **220,** L49.
Elsasser, H. & Staude, H. J., 1978. *Astr. Astrophys. Lett.*, **70,** 43.
Forrest, W. J. & Shure, M. A., 1986. *Astrophys. J.*, **311,** L81 (FS).
Gething, M. R., Warren-Smith, R. F., Scarrott, S. M. & Bingham, R. G., 1982. **198,** 881.
Hoffman, A. W., 1987. In: *Infrared Astronomy with Arrays,* p. 29, eds Wynn-Williams, C. G. & Becklin, E. E., University of Hawaii Press, Hawaii.
Hough, J. H., Sato, S., Tamura, M., Yamashita, T., McFadzean, A. D., Rouse, M. F., Whittet, D. C. B., Kaifu, N., Suzuki, H., Nagata, T., Gatley, I. & Bailey, J., 1988. *Mon. Not. R. astr. Soc.*, **230,** 107.
Hough, J. H., Whittet, D. C. B., Sato, S., Yamashita, T., Tamura, M., Nagata, T., Aitken, D. K. & Roche, P. F., 1989. *Mon. Not. R. astr. Soc.*, **241,** 71 (HEA).
Howell, R. R., McCarthy, D. W. & Low, F. J., 1981. *Astrophys. J. Lett.*, **251,** L21.
Hubble, E. P., 1922. *Astrophys. J.*, **56,** 400.
Johnson, P. E., Rieke, G. M., Lebofsky, M. J. & Kemp, J. C., 1981. *Astrophys. J.*, **245,** 871.
Kaifu, N., 1987. In: *Star Forming Regions, IAU Symp., No. 115,* p. 275, eds Peimbert, M. & Jugku, J., Reidel, Dordrecht.
Lada, C. J., Thronson, H. A., Jr., Smith, H. A., Schwartz, P. R. & Glaccum, W., 1984. *Astrophys. J.*, **286,** 302.
Lonsdale, C. J., Dyck, H. M., Capps, R. W. & Wolstencroft, R. D., 1980. *Astrophys. J. Lett.*, **238,** L31.
Lenzen, R., 1987. *Astr. Astrophys.*, **173,** 124.
McCaughrean, M. J., 1988. *PhD thesis*, University of Edinburgh.
McCaughrean, M. J., 1989. In: *Proceedings of the 3rd Nasa Ames Infrared Detector Technology Workshop, NASA TM 102209,* p. 201, ed. McCreight, C. R.
McLean, I. S., 1987, In: *Infrared Astronomy with Arrays*, p. 180, eds Wynn-Williams, C. G. & Becklin, E. E., University of Hawaii Press, Hawaii.
Minchin, N. R., Hough, J. H., McCall, A., Burton, M. G., McCaughrean, M. J., Aspin, C., Bailey, J., Axon, D. J. & Sato, S., 1990. *Mon. Not. R. astr. Soc.*, **248,** 715 (Paper I).
Orias, G., Hoffman, A. W. & Casselmann, M., 1986. In: *Instrumentation in Astronomy VI, Proc. SPIE*, **627,** 408.
Pendleton, Y. J., Tielens, A. G. G. M. & Werner, M. W., 1990. *Astrophys. J.*, **349,** 107.
Pudritz, R. & Norman, C. A., 1983. *Astrophys. J.*, **274,** 677.
Rayner, J., McLean, I. S., McCaughrean, M. J. & Aspin, C. A., 1989. *Mon. Not. R. astr. Soc.*, **241,** 469.
Rolph, C. D. & Scarrott, S. M., 1988. *Mon. Not. R. astr. Soc.*, **234,** 719.
Sato, S., Nagata, T., Nakajima, T., Nishida, M., Tanaka, M. & Yamashita, T., 1985. *Astrophys. J.*, **291,** 708.
Scarrott, S. M., Draper, P. W. & Warren-Smith, R. F., 1989. *Mon. Not. R. astr. Soc.*, **237,** 621.
Snell, R. L., Loren, R. B. & Plambeck, R. L., 1980. *Astrophys. J. Lett.*, **239,** L17.

Steenman, H. & The, P. S., 1989. *Astrophys. Space Sci.*, **189,** 189.
Torrelles, J. M., Ho, P. T. P., Rodriguez, L. F. & Canto, J., 1989. *Astrophys. J.*, **343,** 222.
Uchida, Y. & Shibata, K., 1984. *Publs Astr. Soc. Japan*, **36,** 105.
Uchida, Y., Kaifu, N., Shibata, K., Hayashi, S. S. & Hasegawa, T., 1987. In: *Star Forming Regions, IAU Symp. No. 115*, p. 287, eds Peimbert, M. & Jugku, J., Reidel, Dordrecht.
Warren-Smith, R. F., Draper, P. W. & Scarrott, S. M., 1987. *Mon. Not. R. astr. Soc.*, **227,** 749.
Ward-Thompson, D., Warren-Smith, R. F., Scarrott, S. M. & Wolstencroft, R. D., 1985. *Mon. Not. R. astr. Soc.*, **215,** 537.
White, G. J., Little, L. T., Parker, E. A., Nicholson, E. S., MacDonald, G. H. & Bale, F., 1975. *Mon. Not. R. astr. Soc.*, **170,** 37P.
Willner, S. P., *et al.*, 1982. *Astrophys. J.*, **253,** 174.
Yamashita, T., Sato, S., Tamura, M., Suzuki, H., Kaifu, N., Takano, T., Mountain, C. M., Moore, T. J. T., Gatley, T. & Hough, J. H., 1987. *Publs Astr. Soc. Japan,* **39,** 809.